Vortex dynamics, pinning, and angle-dependent motion on moiré patterns

Wenzhao Li,[1] C. J. O. Reichhardt,[2] B. Jankó,[1] and C. Reichhardt[2]
[1]Department of Physics, University of Notre Dame, Notre Dame, Indiana 46656, USA
[2]Theoretical Division and Center for Nonlinear Studies, Los Alamos National Laboratory, Los Alamos, New Mexico 87545, USA

(Received 17 December 2020; revised 1 July 2021; accepted 1 July 2021; published 15 July 2021)

We examine the pinning and dynamics of Abrikosov vortices interacting with pinning centers placed in a moiré pattern for varied moiré lattice angles. We find a series of locking angles at which the critical current shows a pronounced dip corresponding to lattices in which the vortices can flow along quasi-one-dimensional channels. At these locking angles, the vortices move with a finite Hall angle. Additionally, for some lattice angles there are peaks in the critical current produced when the substrate has a quasiperiodic character that strongly reduces the vortex channeling. Our results should be general to a broad class of particlelike assemblies moving on moiré patterns.

DOI: 10.1103/PhysRevB.104.024504

I. INTRODUCTION

Moiré patterns are produced by the interference effects that occur when two identical lattices are placed on top of each other and then one of the lattices is shifted or rotated [1,2]. In condensed matter systems, such patterns can appear in a double layer system when one layer is rotated with respect to the other. For certain rotation angles, large scale superlattice ordering occurs that can strongly affect the electronic properties, as found in bilayer graphene [3–5]. Here, we present a study of the pinning and dynamics of assemblies of particles interacting with moiré pinning patterns. We find that, as the moiré pattern is varied, qualitatively new transport patterns emerge for certain *locking* twist angles, giving rise to enhanced longitudinal and transverse (Hall) particle currents.

One of the most ideal systems for studying pinning and sliding dynamics on different types of pattered substrates is vortices in type-II superconductors. In this system, a variety of nanostructuring techniques can be used to realize different pinning array geometries including square [6–12], triangular [8,11,13], rectangular [14–16], diluted [17,18], quasicrystalline [19,20], frustrated [21–23], conformal crystal [24,25], and other structures [26]. The pinning and dynamics can be measured by examining the critical current and transport curves or by direct imaging of the vortex configurations or trajectories. Many of the results found for vortex pinning and motion can also be generalized to other particlelike systems interacting with ordered substrates, such as vortices in Bose-Einstein condensates [27], colloidal assemblies [28–31], skyrmions [32], and frictional systems [33].

A variety of bilayer materials exist that can support superconducting vortices which interact with what is effectively a moiré substrate. It would be interesting to understand if such a system can exhibit a spontaneous Hall angle for the vortex motion, the nature of the vortex movement, and how the critical current might differ for different driving directions. Several recent works have examined skyrmions on moiré patterns [34–36] and these systems could exhibit depinning under a drive. Since skyrmions and vortices have many similarities, their behavior on a moiré pinning array may also show similarities.

Moiré substrates are of interest since they permit the coexistence of multiple length scales even though the individual pinning sites in each layer have only a single length scale. A variety of novel sliding states could arise due to the multiple symmetry directions, making it possible for superconducting vortices to flow in the direction of driving or along one of the symmetry directions of the moiré lattice. Similar effects could occur for any type of particle-based system driven over a moiré substrate. It should be possible to create a variety of different moiré patterns in superconductors using currently existing nanostructuring techniques that have already been employed to generate conformal, periodic, and quasiperiodic pinning arrays. For the latter pinning geometries, predictions from simulations and theory were confirmed in multiple experiments.

In a superconducting vortex system, the pinning properties are typically examined as a function of the magnetic field by varying the number of vortices on a fixed number of pinning sites. For vortices interacting with a moiré pinning array, an additional parameter is important beyond the vortex and pinning density: the angle θ between the two lattices that make up the moiré pattern. Here, we examine vortex pinning and motion in a system with moiré pinning composed from two triangular pinning lattices rotated by an angle θ with respect to each other. As a function of θ, we observe a rich variety of pinning and vortex dynamics that are associated with dips and peaks in the critical current. At commensurate angles where an ordered interference pattern appears, the critical current exhibits a series of dips, and the vortices flow in ordered quasi-one-dimensional channels. At incommensurate angles, these flow channels break apart. Along the commensurate angles, the vortices develop a finite Hall angle due to the guidance or locking of the vortex motion to the moiré pattern. We also find that for other angles, peaks in the critical current appear when a quasicrystalline structure forms in the pinning lattice which

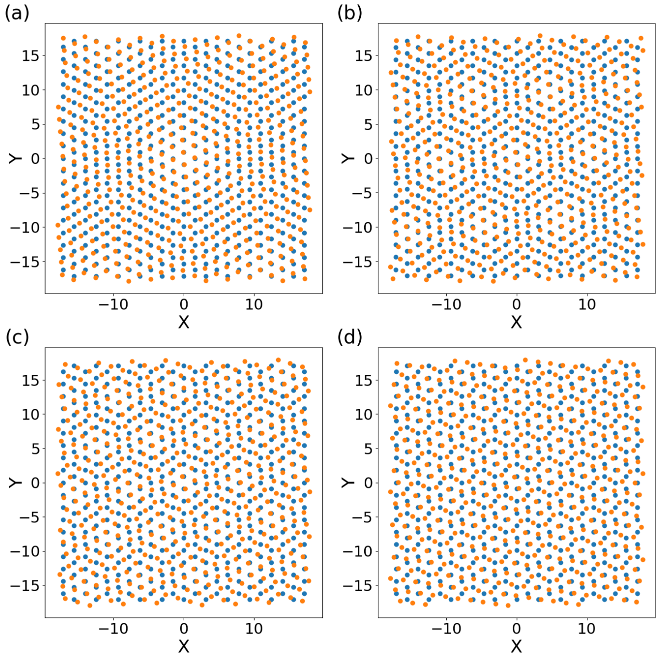

FIG. 1. The pinning array structures for two triangular lattices where the blue lattice is kept fixed and the orange lattice is rotated by an angle θ of (a) 5.0°, (b) 9.4°, (c) 13.2°, and (d) 21.8°.

strongly suppresses easy flow channeling of the vortices. As a greater number of van der Waals type systems are studied, a number of cases could arise in which depinning, friction, flow, and pinning on a moiré substrate could arise. Our results are of interest for understanding the flow of vortices, colloidal particles, skyrmions, and Wigner crystals on such moiré substrates.

II. SIMULATION

We model a system of N_v vortices interacting with a moiré pattern of pinning sites. The equation of motion for vortex i is given by

$$\eta\frac{d\mathbf{R}}{dt} = \mathbf{F}_i^{vv} + \mathbf{F}_i^{p} + \mathbf{F}^{d} + \mathbf{F}_i^{T}. \quad (1)$$

Here, $\eta = 1$ is the damping coefficient and the time step is set to $dt = 0.008$. The repulsive vortex-vortex interaction force has the form $\mathbf{F}_i^{vv} = \sum F_0 K_1(R_{ij}/\lambda)\hat{\mathbf{R}}_{ij}$, where K_1 is the modified Bessel function, R_{ij} is the distance between vortex i and vortex j, $F_0 = \phi_0^2/2\pi\mu_0\lambda^3 = 8.0/\lambda^3$, and λ is the penetration depth which we set equal to $\lambda = 1.8$. We consider a system of size $L \times L$ with $L = 20\lambda$ and with periodic boundary conditions in the x and y directions. The vortex density is $n_v = N_v/L^2$. The pinning force is given by $F_i^P = -\sum_{k=1}^{N_p} F_p R_{ik} \exp(-R_{ik}^2/r_p^2)\hat{\mathbf{R}}_{ij}$ where we fix $r_p = 0.6$. The pinning sites are arranged in two identical triangular lattices with a lattice constant of 1.8, and the lattices are rotated with respect to each other by an angle θ. We consider $\theta = 0$ to $\theta = 30^\circ$ in increments of $\delta\theta = 0.1^\circ$. In Fig. 1 we illustrate some representative moiré pinning structures for varied angles $\theta = 5.0^\circ$, 9.4°, 13.2°, and 21.8° between the two lattices, which are colored blue and orange. The pinning sites form a superlattice with a superlattice constant that decreases as θ increases. The thermal forces arise from Langevin kicks with the following properties: $\langle F_i^T(t)\rangle = 0.0$ and $\langle F_i^T(t)F_j^T(t')\rangle = 2\eta k_B T\delta_{ij}\delta(t-t')$. The initial vortex configurations are obtained by starting from a high temperature liquid state and cooling down to 0 K in 80 intervals, where we wait 10^4 time steps during each interval. After annealing we apply a drive in the form of a Lorentz force $F^D = (J \times \hat{\mathbf{z}})\phi_0 d$ which produces vortex motion along the x direction.

We obtain the critical current by measuring the total vortex velocity $V_x = N_t^{-1}\sum_t\sum_i \hat{\mathbf{x}}\cdot\mathbf{v}_i$, where N_t is the total number of time steps and $\mathbf{v}_i$ is the vortex velocity. When V_x exceeds a threshold where nontrivial steady state vortex motion occurs, the system is defined as being depinned. We obtain the depinning force using a binary search technique. The simulations are performed using a parallelized code, and we typically consider 3000 configurations for each of 300 different values of θ and ten different vortex densities. Some representative annealed vortex configurations for varied vortex densities and θ appear in Fig. 2 for a sample with 100 vortices at $n_v = 0.25$, in Fig. 3 for a sample with 300 vortices at $n_v = 0.75$, and in Fig. 4 for a sample with 1000 vortices at $n_v = 2.5$.

III. RESULTS

In Fig. 5(a) we plot the critical current F_c vs θ for the system in Fig. 1 at vortex densities of $n_v = 0.25$–2.5 in increments of 0.25. Here, the overall critical current decreases with increasing vortex density and there are a series of dips

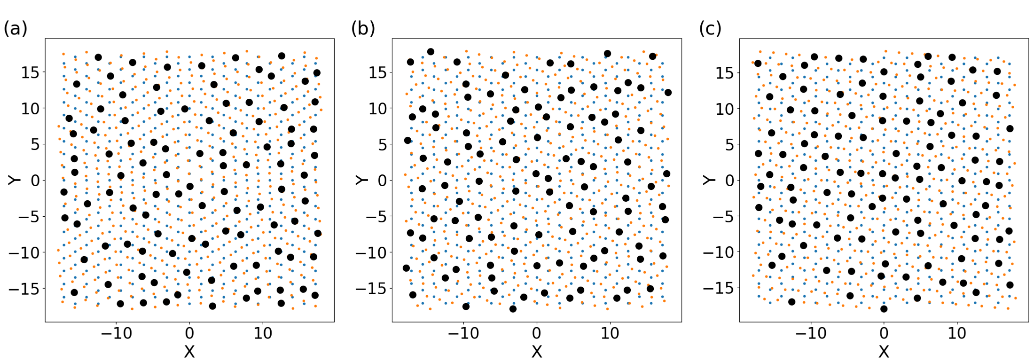

FIG. 2. Vortex configurations after annealing for a system with 100 vortices (density $n_v = 0.25$) for (a) $\theta = 5^\circ$, (b) 15°, and (c) 25°. Blue dots: Pinning site centers for a hexagonal lattice. Orange dots: A second hexagonal lattice rotated by θ. Large dots: Vortices.

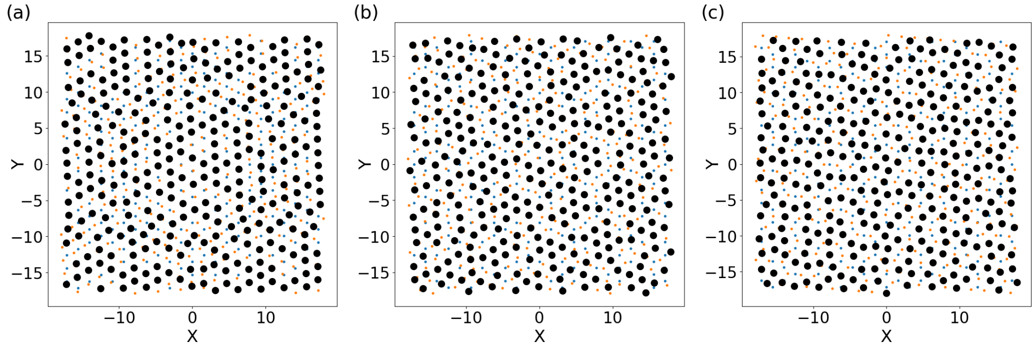

FIG. 3. Vortex configurations after annealing for a system with 300 vortices ($n_v = 0.75$) for (a) $\theta = 5^\circ$, (b) 15°, and (c) 25°. Blue dots: Pinning site centers for a hexagonal lattice. Orange dots: A second hexagonal lattice rotated by θ. Large dots: Vortices.

at specific angles. The initial peak in F_c at $\theta = 0.0^\circ$ appears when the pinning sites form a triangular lattice. We have also tested these results for different system sizes and we find that the angles at which the dips and peaks occur are insensitive to system size, as shown in Fig. 6.

Figure 5(b) shows F_c vs θ for the samples with $n_v = 1.25$, where dips in F_c appear at $\theta = 9.4^\circ$, 13.2°, and 21.8°. In a moiré pattern formed from two triangular lattices, ordered or commensurate structures occur at the following angles [5,37],

$$\cos(\theta) = \frac{3p^2 + 3pq + q^2/2}{3p^2 + 3pq + q^2}, \tag{2}$$

where p and q are integers. The values $p = 1$ and $q = 1$ correspond to $\theta = 21.786^\circ$, $p = 2$ and $q = 1$ correspond to $\theta = 13.7^\circ$, and $p = 3, q = 1$ correspond to $\theta = 9.4^\circ$. The dips we observe in the critical current match these commensurate angles. Due to the symmetry of the system, the features in Fig. 5 repeat in the range $\theta = 30^\circ$–60°.

In Fig. 5(b), letters highlight the values of θ at which the vortices are just able to depin, as illustrated in Fig. 7, where the color code corresponds to different times. Figure 7(a) shows the trajectories at $\theta = 9.4^\circ$ and $F_d = 1.5$, where the vortices flow in a series of quasi-one-dimensional channels along the edges of the superlattice. In Fig. 7(b), at $\theta = 13.2^\circ$ and $F_d = 1.5$, a similar set of trajectories form in which the motion follows the superlattice edge. Since the superlattice spacing decreases with increasing θ, the number of possible quasi-one-dimensional channels for motion increases with increasing θ. In Fig. 7(c), the trajectories at a noncommensurate angle of $\theta = 17^\circ$ and $F_d = 2.0$ are much more disordered. At $\theta = 21.8^\circ$ and $F_d = 1.5$ in Fig. 7(d), the vortex motion again follows well-defined channels. In general, the flow at incommensurate angles has reduced channeling compared to the flow at commensurate angles.

In addition to dips at the commensurate angles, we also find peaks in F_c in Fig. 5. The most prominent peak of this type occurs near $\theta = 27.9^\circ$ for vortex densities near $n_v = 1.25$. In Fig. 8(a) we illustrate the pinning site configurations at this angle, where we find features such as fivefold ordering similar to those observed in quasicrystals. Figure 8(b) shows that the vortex trajectories over this substrate just above depinning have strongly reduced channeling. For triangular moiré patterns, the most incommensurate angle corresponds to $\theta = 30^\circ$ [5]. In our system we generally find a small dip in the critical current when $\theta = 30^\circ$, while the peak in F_c falls at $\theta = 27.9^\circ$ The downward shift of the peak location could be a result of the finite size of the pinning sites or of the vortex-vortex interactions which can produce a collectively moving state.

When vortex channeling occurs, we find a finite Hall effect or transverse motion due to the fact that the easy flow channels are at an angle to the driving direction, as shown in Fig. 7. In Fig. 9 we plot $\langle V_y \rangle$ vs θ for the system in Fig. 5(b) at $F_d = 1.5$, 2.0, 2.5, and 3.0. Peaks in the Hall velocity appear at $\theta = 21.8^\circ$ and 13.7°, with a weaker channeling effect at $\theta = 9.4^\circ$. There is also an extended region from $12^\circ < \theta < 23^\circ$ in which some biased flow in the y direction occurs as F_d increases. The vortex flow is generally more ordered for

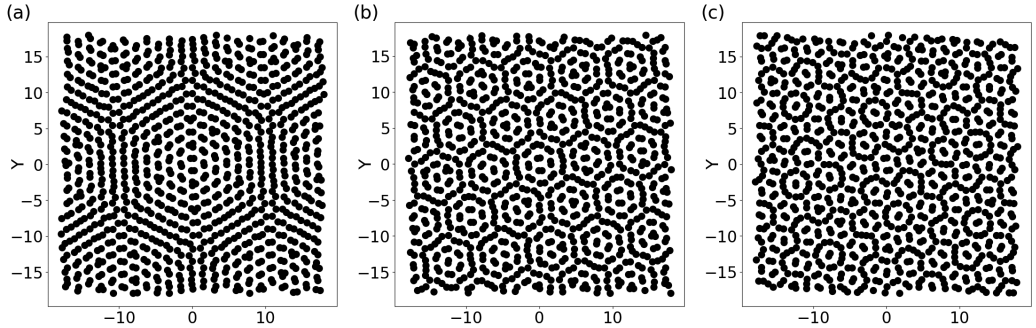

FIG. 4. Vortex configurations after annealing for a system with 1000 vortices ($n_v = 2.5$) for (a) $\theta = 5^\circ$, (b) 15°, and (c) 25°. Blue dots: Pinning site centers for a hexagonal lattice. Orange dots: A second hexagonal lattice rotated by θ. Large dots: Vortices.

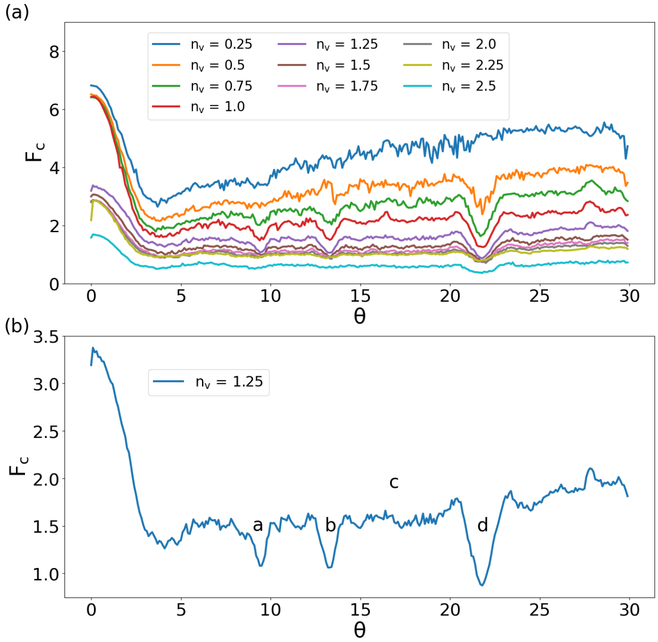

FIG. 5. (a) The critical current F_c vs θ for the system in Fig. 1 at varied vortex densities of $n_v = 0.25$–2.5 in increments of 0.25. (b) F_c vs θ at $n_v = 1.25$, showing dips at $\theta = 9.4^\circ$, 13.2°, and 21.8° as well as a peak near 28°. The letters a, b, c, and d correspond to the locations of the images in Fig. 7.

$\theta < 12^\circ$ even at incommensurate angles since the vortices follow large scale zigzag patterns, as is shown for $\theta = 6.6^\circ$ in Fig. 10. Experimentally it is possible to measure transverse vortex motion with various techniques [38,39]. Although we find strong variations in the critical current as a function of the angle θ, we do not observe pronounced features as a function of field. Instead, F_c generally decreases smoothly with

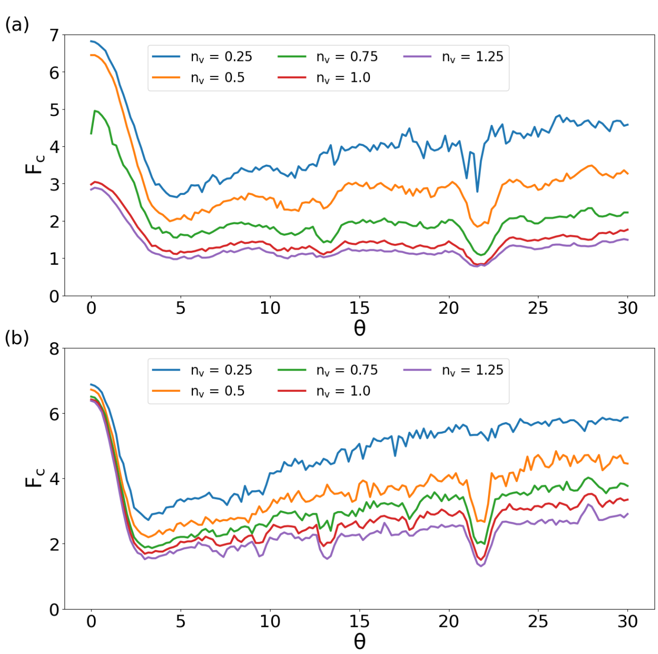

FIG. 6. Critical current F_c vs θ in samples of size (a) $L = 16\lambda$ and (b) $L = 24\lambda$.

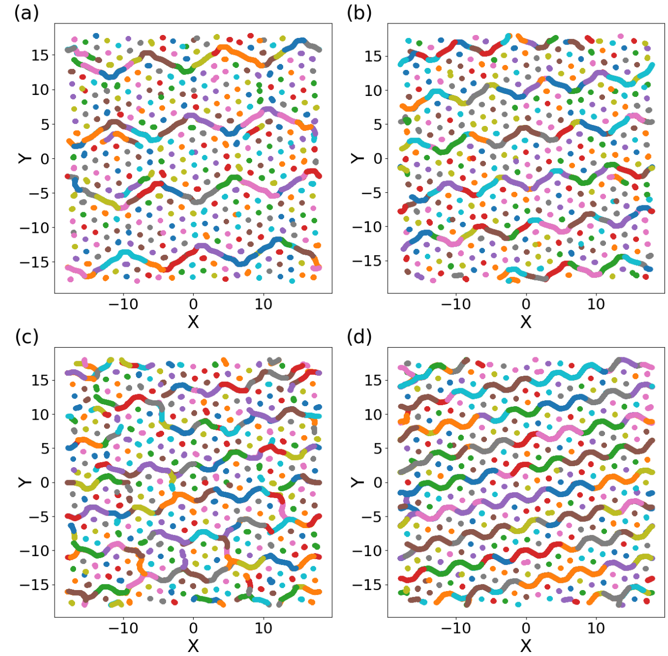

FIG. 7. The vortex positions (dots) and trajectories (lines) just above depinning for the system in Fig. 5(b) with $n_v = 1.25$. Different colors indicate the motion of different individual vortices. (a) $\theta = 9.4^\circ$ and $F_d = 1.5$, where quasi-one-dimensional flow patterns form. (b) $\theta = 13.2^\circ$ and $F_d = 1.5$, with easy flow channeling. (c) $\theta = 17^\circ$ and $F_d = 2.0$, an incommensurate angle showing more disordered channeling. (d) $\theta = 21.8^\circ$ and $F_d = 1.5$, where there is strong channeling.

increasing n_v except for a jump down when the number of vortices crosses from less to more than the number of pinning sites, as shown in Fig. 11.

The presence of anisotropy and Hall transport is a direct consequence of the geometrical moiré pattern, emerging from the two rotated triangular lattices, which allows certain easy flow directions to arise that do not necessary align with the direction of drive. This effect can also occur for systems

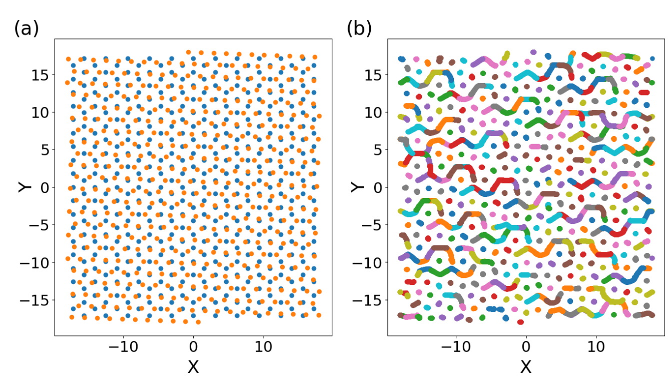

FIG. 8. (a) The pinning site arrangement for the system in Fig. 5(b) at $\theta = 27.9^\circ$ where a peak appears in the critical current near $n_v = 1.25$. Here, the substrate has considerable fivefold ordering or quasiperiodic type ordering. (b) The vortex flow pattern over the pinning sites at $F_D = 2.0$, showing a lack of ordered motion. Different colors indicate the motion of different individual vortices.

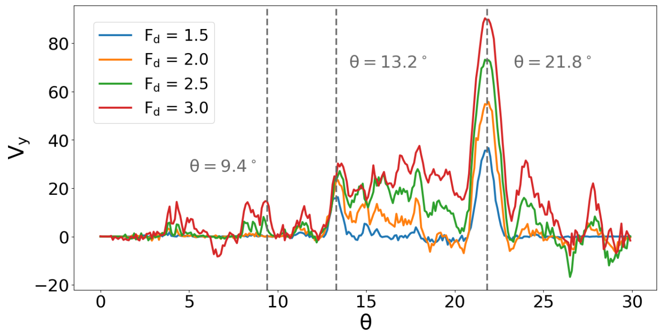

FIG. 9. The transverse velocity $\langle V_y \rangle$ vs θ for the system in Fig. 5(b) at $F_d = 1.5$, 2.0, 2.5, and 3.0, from bottom to top. There are strong transverse velocities at the commensurate angles, which correspond to the dips in the critical current.

with only a single periodic substrate lattice, such as a triangular lattice where the motion can follow the easy flow directions of 30° or 60° [40,41]. In the case of the moiré substrate, the locking angles serve as easy flow directions for vortex motion. Directional locking can also be observed by rotating the direction of drive and observing the enhanced locking flow when the drive matches these locking angles. Some experimental geometries that could be used to measure the transverse voltage include cross-shaped contacts of the type used for studying vortex flow over periodic pinning [38,42,43]. It is also possible that at high drives, the driving force would overwhelm the substrate energy and the transverse response would drop as the vortices begin to move along the driving direction instead of along the locking angles.

Our results could be tested using vortices on nanopatterned arrays or for pinning sites created using multiple Bitter decorations [44]. They could also be applied to colloids interacting with optical traps, where it would be possible to change θ

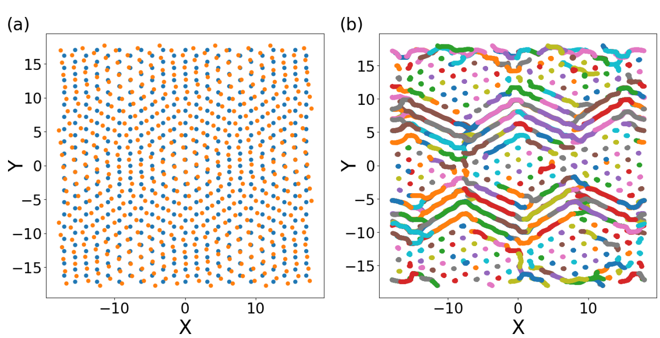

FIG. 10. Vortex trajectories at $\theta = 6.6°$, $n_v = 1.25$, and $F_d = 3.0$.

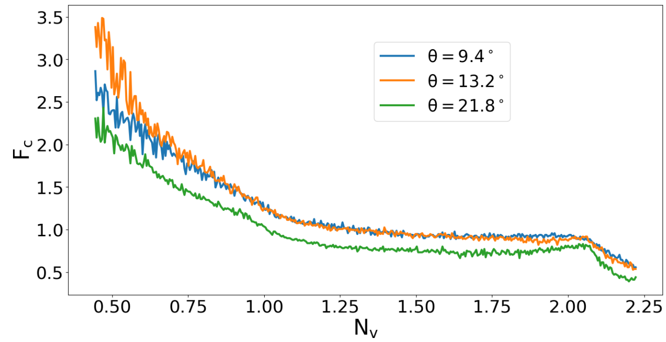

FIG. 11. Critical current F_c vs magnetic field n_v for $\theta = 9.4°$, 13.2°, and 21.8°. There is a drop in F_c when $N_v/N_p > 2.0$.

as a function of time. Additionally, there are proposals that the insulating state in some bilayer systems consists of a Wigner crystal that could undergo depinning transitions in which the threshold could exhibit dips at the commensurate angles [45,46].

IV. SUMMARY

We have examined the pinning and dynamics of vortices interacting with a moiré pattern consisting of two triangular pinning lattices that are rotated with respect to each other. We find a series of dips in the critical current corresponding to commensurate locking angles where the system forms an ordered superlattice and the vortices follow easy flow quasi-one-dimensional channels. We also find that for some incommensurate angles, the substrate has a quasicrystalline structure and there is a peak in the critical current due to the suppression of vortex channeling. Dips in the critical current are correlated with the appearance of a finite Hall angle for the vortex motion when the channeling motion occurs at an angle with respect to the driving direction. Our results could be tested for vortices or colloids on moiré substrates.

ACKNOWLEDGMENTS

We gratefully acknowledge the support of the US Department of Energy through the LANL/LDRD program for this work. This work was supported by the US Department of Energy through the Los Alamos National Laboratory. Los Alamos National Laboratory is operated by Triad National Security, LLC, for the National Nuclear Security Administration of the US Department of Energy (Contract No. 892333218NCA000001). W.L. and B.J. were supported in part by NSF, Grant No. DMR-1952841.

[1] K. Kobayashi, Moiré pattern in scanning tunneling microscopy: Mechanism in observation of subsurface nanostructures, Phys. Rev. B **53**, 11091 (1996).

[2] H. Miao, A. Panna, A. A. Gomella, E. E. Bennett, S. Znati, L. Chen, and H. Wen, A universal moiré effect and application in X-ray phase-contrast imaging, Nat. Phys. **12**, 830 (2016).

[3] S. Shallcross, S. Sharma, E. Kandelaki, and O. A. Pankratov, Electronic structure of turbostratic graphene, Phys. Rev. B **81**, 165105 (2010).

[4] Y. Cao, V. Fatemi, S. Fang, K. Watanabe, T. Taniguchi, E. Kaxiras, and P. Jarillo-Herrero, Unconventional superconductivity in magic-angle graphene superlattices, Nature (London) **556**, 43 (2018).

[5] W. Yao, E. Wang, C. Bao, Y. Zhang, K. Zhang, K. Bao, C. K. Chan, C. Chen, J. Avila, M. C. Asensio, J. Zhu, and S. Zhou, Quasicrystalline 30° twisted bilayer graphene as an incommensurate superlattice with strong interlayer coupling, Proc. Natl. Acad. Sci. USA **115**, 6928 (2018).

[6] M. Baert, V. V. Metlushko, R. Jonckheere, V. V. Moshchalkov, and Y. Bruynseraede, Composite Flux-Line Lattices Stabilized in Superconducting Films by a Regular Array of Artificial Defects, Phys. Rev. Lett. **74**, 3269 (1995).

[7] K. Harada, O. Kamimura, H. Kasai, T. Matsuda, A. Tonomura, and V. V. Moshchalkov, Direct observation of vortex dynamics in superconducting films with regular arrays of defects, Science **274**, 1167 (1996).

[8] C. Reichhardt, C. J. Olson, and F. Nori, Commensurate and incommensurate vortex states in superconductors with periodic pinning arrays, Phys. Rev. B **57**, 7937 (1998).

[9] V. Metlushko, U. Welp, G. W. Crabtree, R. Osgood, S. D. Bader, L. E. DeLong, Z. Zhang, S. R. J. Brueck, B. Ilic, K. Chung, and P. J. Hesketh, Interstitial flux phases in a superconducting niobium film with a square lattice of artificial pinning centers, Phys. Rev. B **60**, R12585 (1999).

[10] A. N. Grigorenko, S. J. Bending, M. J. Van Bael, M. Lange, V. V. Moshchalkov, H. Fangohr, and P. A. J. de Groot, Symmetry Locking and Commensurate Vortex Domain Formation in Periodic Pinning Arrays, Phys. Rev. Lett. **90**, 237001 (2003).

[11] G. R. Berdiyorov, M. V. Milošević, and F. M. Peeters, Novel Commensurability Effects in Superconducting Films with Antidot Arrays, Phys. Rev. Lett. **96**, 207001 (2006).

[12] A. Crassous, R. Bernard, S. Fusil, K. Bouzehouane, D. Le Bourdais, S. Enouz-Vedrenne, J. Briatico, M. Bibes, A. Barthélémy, and J. E. Villegas, Nanoscale Electrostatic Manipulation of Magnetic Flux Quanta in Ferroelectric/Superconductor $BiFeO_3/YBa_2Cu_3O_{7-\delta}$ Heterostructures, Phys. Rev. Lett. **107**, 247002 (2011).

[13] J. I. Martín, M. Vélez, J. Nogués, and I. K. Schuller, Flux Pinning in a Superconductor by an Array of Submicrometer Magnetic Dots, Phys. Rev. Lett. **79**, 1929 (1997).

[14] J. I. Martín, M. Vélez, A. Hoffmann, I. K. Schuller, and J. L. Vicent, Artificially Induced Reconfiguration of the Vortex Lattice by Arrays of Magnetic Dots, Phys. Rev. Lett. **83**, 1022 (1999).

[15] G. Karapetrov, J. Fedor, M. Iavarone, D. Rosenmann, and W. K. Kwok, Direct Observation of Geometrical Phase Transitions in Mesoscopic Superconductors by Scanning Tunneling Microscopy, Phys. Rev. Lett. **95**, 167002 (2005).

[16] C. J. Olson Reichhardt, A. Libál, and C. Reichhardt, Vortex configurations and dynamics in elliptical pinning sites for high matching fields, Phys. Rev. B **73**, 184519 (2006).

[17] C. Reichhardt and C. J. Olson Reichhardt, Commensurability effects at nonmatching fields for vortices in diluted periodic pinning arrays, Phys. Rev. B **76**, 094512 (2007).

[18] M. Kemmler, D. Bothner, K. Ilin, M. Siegel, R. Kleiner, and D. Koelle, Suppression of dissipation in Nb thin films with triangular antidot arrays by random removal of pinning sites, Phys. Rev. B **79**, 184509 (2009).

[19] V. Misko, S. Savel'ev, and F. Nori, Critical Currents in Quasiperiodic Pinning Arrays: Chains and Penrose Lattices, Phys. Rev. Lett. **95**, 177007 (2005).

[20] M. Kemmler, C. Gürlich, A. Sterck, H. Pöhler, M. Neuhaus, M. Siegel, R. Kleiner, and D. Koelle, Commensurability Effects in Superconducting Nb Films with Quasiperiodic Pinning Arrays, Phys. Rev. Lett. **97**, 147003 (2006).

[21] A. Libál, C. J. Olson Reichhardt, and C. Reichhardt, Creating Artificial Ice States using Vortices in Nanostructured Superconductors, Phys. Rev. Lett. **102**, 237004 (2009).

[22] M. L. Latimer, G. R. Berdiyorov, Z. L. Xiao, F. M. Peeters, and W. K. Kwok, Realization of Artificial Ice Systems for Magnetic Vortices in a Superconducting MoGe Thin Film with Patterned Nanostructures, Phys. Rev. Lett. **111**, 067001 (2013).

[23] J.-Y. Ge, V. N. Gladilin, J. Tempere, V. S. Zharinov, J. Van de Vondel, J. T. Devreese, and V. V. Moshchalkov, Direct visualization of vortex ice in a nanostructured superconductor, Phys. Rev. B **96**, 134515 (2017).

[24] D. Ray, C. J. Olson Reichhardt, B. Jankó, and C. Reichhardt, Strongly Enhanced Pinning of Magnetic Vortices in Type-II Superconductors by Conformal Crystal Arrays, Phys. Rev. Lett. **110**, 267001 (2013).

[25] Y. L. Wang, M. L. Latimer, Z. L. Xiao, R. Divan, L. E. Ocola, G. W. Crabtree, and W. K. Kwok, Enhancing the critical current of a superconducting film in a wide range of magnetic fields with a conformal array of nanoscale holes, Phys. Rev. B **87**, 220501(R) (2013).

[26] I. A. Sadovskyy, A. E. Koshelev, W.-K. Kwok, U. Welp, and A. Glatz, Targeted evolution of pinning landscapes for large superconducting critical currents, Proc. Natl. Acad. Sci. USA **116**, 10291 (2019).

[27] S. Tung, V. Schweikhard, and E. A. Cornell, Observation of Vortex Pinning in Bose-Einstein Condensates, Phys. Rev. Lett. **97**, 240402 (2006).

[28] K. Mangold, P. Leiderer, and C. Bechinger, Phase Transitions of Colloidal Monolayers in Periodic Pinning Arrays, Phys. Rev. Lett. **90**, 158302 (2003).

[29] T. Bohlein, J. Mikhael, and C. Bechinger, Observation of kinks and antikinks in colloidal monolayers driven across ordered surfaces, Nat. Mater. **11**, 126 (2012).

[30] A. Vanossi, N. Manini, and E. Tosatti, Static and dynamic friction in sliding colloidal monolayers, Proc. Natl. Acad. Sci. USA **109**, 16429 (2012).

[31] D. McDermott, J. Amelang, C. J. Olson Reichhardt, and C. Reichhardt, Dynamic regimes for driven colloidal particles on a periodic substrate at commensurate and incommensurate fillings, Phys. Rev. E **88**, 062301 (2013).

[32] C. Reichhardt, D. Ray, and C. J. O. Reichhardt, Nonequilibrium phases and segregation for skyrmions on periodic pinning arrays, Phys. Rev. B **98**, 134418 (2018).

[33] A. Vanossi, N. Manini, M. Urbakh, S. Zapperi, and E. Tosatti, Colloquium: Modeling friction: From nanoscale to mesoscale, Rev. Mod. Phys. **85**, 529 (2013).

[34] Q. Tong, F. Liu, J. Xiao, and W. Yao, Skyrmions in the moiré of van der Waals 2D magnets, Nano Lett. **18**, 7194 (2018).

[35] K. Hejazi, Z.-X. Luo, and L. Balents, Heterobilayer moiré magnets: Moiré skyrmions, commensurate-incommensurate transition, arXiv:2009.00860.

[36] M. Akram and O. Erten, Skyrmions in twisted van der Waals magnets, Phys. Rev. B **103**, L140406 (2021).

[37] J. M. B. Lopes dos Santos, N. M. R. Peres, and A. H. Castro Neto, Continuum model of the twisted graphene bilayer, Phys. Rev. B **86**, 155449 (2012).

[38] J. E. Villegas, E. M. Gonzalez, M. I. Montero, I. K. Schuller, and J. L. Vicent, Vortex-lattice dynamics with channeled pinning potential landscapes, Phys. Rev. B **72**, 064507 (2005).

[39] G. Zechner, W. Lang, M. Dosmailov, M. A. Bodea, and J. D. Pedarnig, Transverse vortex commensurability effect and sign change of the Hall voltage in superconducting $YBa_2Cu_3O_{7-\delta}$ thin films with a nanoscale periodic pinning landscape, Phys. Rev. B **98**, 104508 (2018).

[40] C. Reichhardt and C. J. Olson Reichhardt, Spontaneous Transverse Response and Amplified Switching in Superconductors with Honeycomb Pinning Arrays, Phys. Rev. Lett. **100**, 167002 (2008).

[41] R. L. Stoop, A. V. Straube, T. H. Johansen, and P. Tierno, Collective Directional Locking of Colloidal Monolayers on a Periodic Substrate, Phys. Rev. Lett. **124**, 058002 (2020).

[42] A. V. Silhanek, L. Van Look, S. Raedts, R. Jonckheere, and V. V. Moshchalkov, Guided vortex motion in superconductors with a square antidot array, Phys. Rev. B **68**, 214504 (2003).

[43] J. I. Vestgården, V. V. Yurchenko, R. Wördenweber, and T. H. Johansen, Mechanism for flux guidance by micrometric antidot arrays in superconducting films, Phys. Rev. B **85**, 014516 (2012).

[44] Y. Fasano, M. Menghini, F. de la Cruz, and G. Nieva, Weak interaction and matching conditions for replicas of vortex lattices, Phys. Rev. B **62**, 15183 (2000).

[45] B. Padhi, C. Setty, and P. W. Phillips, Doped twisted bilayer graphene near magic angles: proximity to Wigner crystallization, not Mott insulation, Nano Lett. **18**, 6175 (2018).

[46] B. Padhi, R. Chitra, and P. W. Phillips, Generalized Wigner crystallization in moiré materials, Phys. Rev. B **103**, 125146 (2021).